3. POST EARTHQUAKE SEQUENCE LAND DEFORMATION

Land damage from the four largest earthquakes in the 2010-2011 Canterbury earthquake sequence (CES) have been well documented in previous GEER reports and by numerous researchers (e.g., Quigley et al., 2010; Quigley et al. 2013; Cubrinovski et al., 2014; Green et al., 2014; Maurer et al., 2014; van Ballegooy et al., 2014). The effects of tectonic uplift, liquefaction induced settlement, sedimentation of river channels from ejected material and lateral spreading has resulted in land damage and influenced river morphology within Christchurch. The GEER team specifically investigated the related land damage mechanisms and their impacts on the March 5th flood event. The impacts of the land damage and changes in the river are summarized in this section.

Tectonic uplift and earthquake shaking

Earthquake frequency-magnitude distributions during the CES are summarized in Figure 3-1 and Figure 3-2 (Li et al., 2013; Bradley et al., 2014; Quigley et al., in review). The eight largest earthquakes by magnitude include the 4 September 2010 (Mw=7.1), 22 February 2011 (three earthquakes: Mw=6.2, 5.5, 5.6), 13 June 2011 (two earthquakes: Mw=5.3, 6.0) and 23 December 2011 (two earthquakes: Mw=5.8, 5.9). Figure 3-1B shows how all of these earthquakes were accompanied by an increase in aftershock frequency (Figure 3-1B). Figure 3-3 presents the magnitudes weighted (to Mw7.5) peak ground accelerations (PGA7.5). As seen in Figure 3-3, all of the Mw $\geq$ 5.8 events, and the Mw 5.3 June event, caused ground shaking in eastern and southern Christchurch with PGA7.5 $\geq$ 0.10g , and caused significant liquefaction damage, as indicated by the formation of sand blows and lateral spreading cracks in the most susceptible parts of eastern Christchurch (e.g., Quigley et al., 2013). Spatially localized, minor liquefaction was also reported in isolated areas following the 19 Oct 2010 Mw 4.8 (Green et al., 2010), 16 April 2011 Mw 5.0, and 21 June 2011 Mw 5.2 earthquakes (Quigley et al., 2013), although these events did not cause significant land damage and are thus unlikely to have contributed to increased flood hazard. The locations of major faults involved in the CES are shown in Figure 3-2. For detailed reviews of the geologic and seismic aspects of the CES see Quigley et al. (2010, 2012, 2013); Beavan et al. (2010, 2011, 2012), Kaiser et al. (2011); Duffy et al. (2012), Bradley et al. (2014); and Hughes et al. (in review). No pre-CES regional earthquakes since 1940 are likely to have been of sufficient magnitude and shaking intensity to induce liquefaction and impact on flood hazard (Figure 3-1A). A local earthquake (Mw 4.7-4.9) in 1869 caused pervasive damage in parts of Christchurch consistent with PGA $\geq$ 0.2 g shaking and may have induced tidal changes in the Heathcote River, as reported in the Weekly News 26 June 1869 (cited in Downes and Yetton, 2012).

Vertical tectonic surface displacements of 0.8 to 1.8 m along the Greendale Fault approximately 50 km west of Christchurch caused partial avulsion of the Hororata River shown in Figure 3-2

and related flooding (Duffy et al., 2013) during the 4 Sept 2010 earthquake. However, vertical deformations in Christchurch (excluding the effects of lateral spreading and liquefaction) in this event were < 2-5 cm (Beavan et al., 2010, 2012) and thus did not contribution significantly to flood hazard.

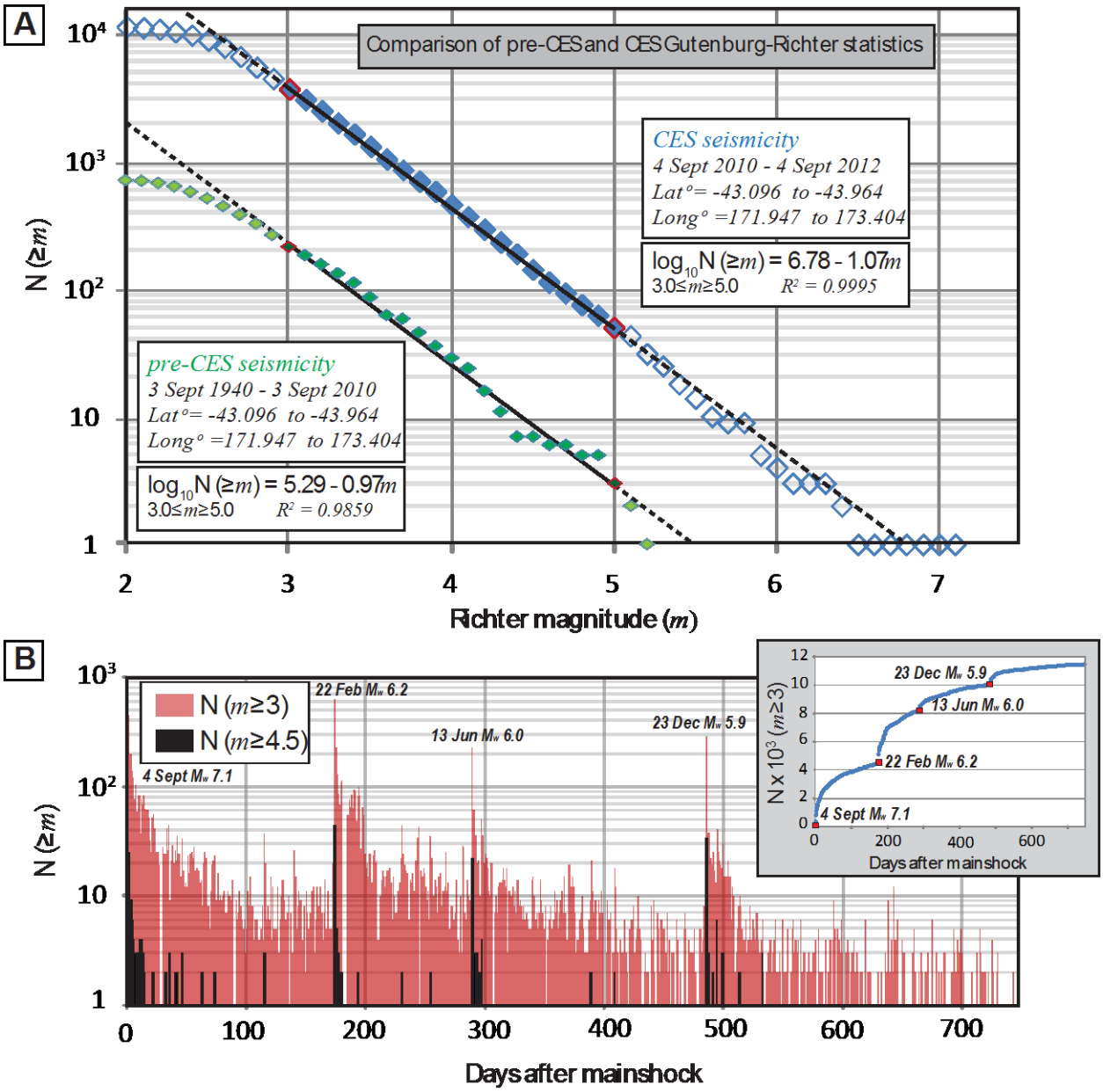

Figure 3-1 Seismicity of the Canterbury earthquake sequence (CES). A) Gutenburg-Richter frequency-magnitude plot comparing CES seismicity with seismicity in the same region over a 60 year period prior to the CES. The low earthquake frequency and magnitudes prior to the CES suggests that regional earthquakes over this time period are unlikely to have contributed to flood hazard via seismic shaking. See text for additional details. B) CES earthquakes plotted against time, showing increase in seismicity rate immediately following larger (e.g., Mw ≥ 5.5) events and decay of seismicity rates following these events (inset).

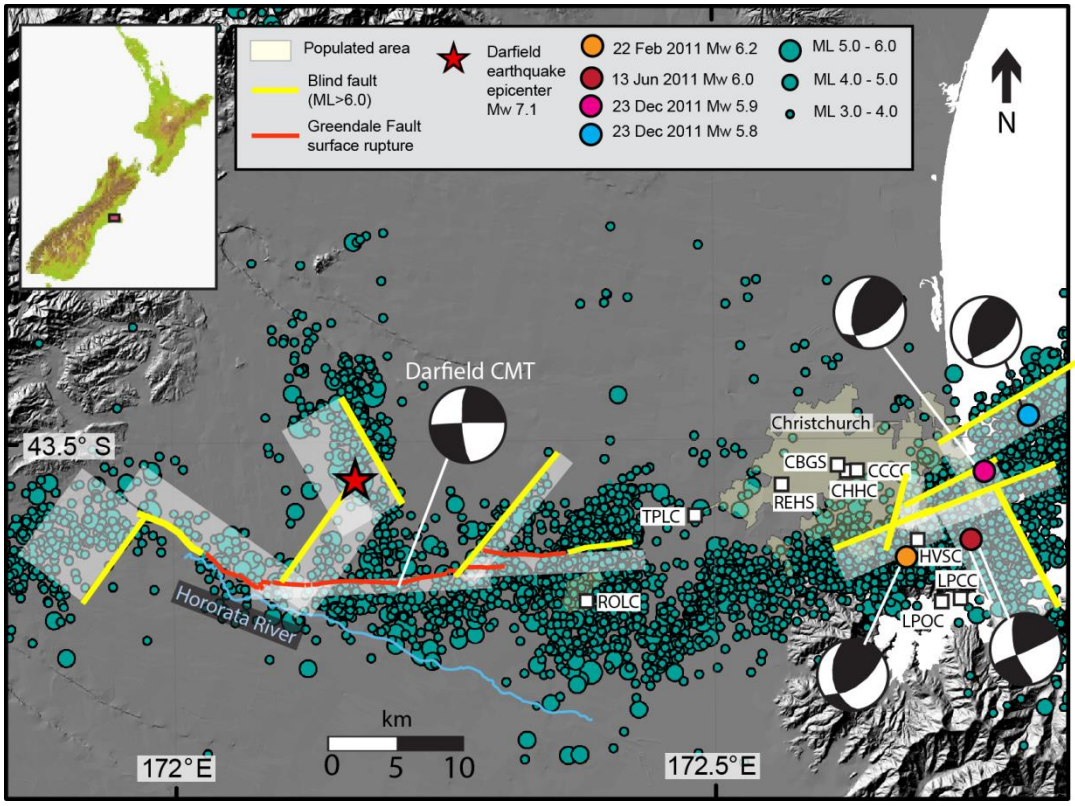

Figure 3-2 Location of active faults that ruptured in the CES and related spatial distribution of Richter magnitude (ML) ≥ 3.0 earthquakes. Focal mechanisms for major events as shown. Of the estimated 12 to 14 major faults that ruptured in the CES, only two faults (Greendale Faults east/central and west) caused surface rupture; the rest of the faults were blind.

The 22 February 2011 Mw 6.2 Christchurch earthquake involved the rupture of 2 to 3 blind faults, shown in Figure 3-2 and Figure 3-4, with reverse and right-lateral displacements (Beavan et al. 2012). The inferred rupture reached as shallow as ~0.5 km depth below the surface, suggesting rupture termination in Miocene volcanic rocks. Maximum coseismic slip was 2.5 to 3 m at depths of 4-6 km (Beavan et al. 2012). Constraints on surface deformation above the fault ruptures are provided by continuous GPS (cGPS), geodetic 'campaign' GPS, differential Interformetric Synthetic Aperture Radar (InSAR), and differential Light Detection and Ranging (LiDAR) data. Maximum vertical displacements recorded by cGPS in the Christchurch earthquake were -51 mm at TNZ (Figure 3-4A); no cGPS vertical displacements in the other earthquakes exceeded 10 mm (Beavan et al., 2012) and thus this data is not considered further. Maximum 22 February earthquake vertical displacements recorded by campaign GPS data include 535 mm uplift near the Avon Heathcote Estuary (open star in Figure 3-4A) and numerous locations with ≥ 100 mm of subsidence (Figure 3-4A); Beavan et al. (2011) cautioned that large errors may be associated with some of these data. Differential InSAR reveals large (> 6-10 km^2) areas of ≥30 cm displacement towards and away from satellite look directions (Beavan et al., 2011) that reflect both horizontal and vertical displacements resulting from tectonic and shaking induced deformation. Differential LiDAR reveals areas of vertical uplift

that exceed 30-40 cm and large areas of subsidence of >10-50 cm (Hughes et al., in review). Vertical uplift primarily reflects tectonic displacement on the underlying faults, while subsidence records differential settlement, lateral spreading and other types of ground failure in addition to tectonic displacement variations.

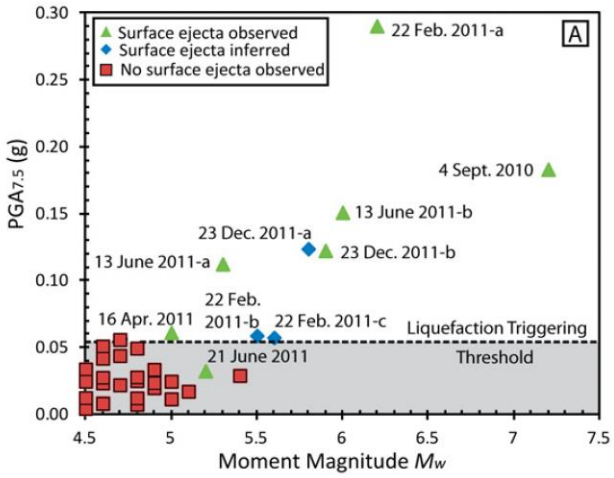

Figure 3-3 Relationship of magnitude-weighted PGA7.5 and Mw for largest CES earthquakes that did and did not create surface evidence for liquefaction at a selected study site adjacent to the Avon River in eastern Christchurch. PGA7.5 thresholds for inducing major liquefaction and lateral spreading at this site are 0.10 g, although surface features were created at shaking intensities as low as ≤ 0.06 g. A shaking threshold ≥ 0.1g PGA7.5 for inducing land damage and influencing channel morphology, flood plain elevations, and consequently flood hazard at high susceptibility sites is likely. Figure from Quigley et al. (2013).

The 13 June 2011 Mw 6.0 earthquake likely involved an intersecting ENE-striking reverse-right lateral fault and NW-striking left-lateral fault, shown in Figure 3-4B with ~ 1 km deep rupture extent and maximum subsurface slip of < 1 m (Beavan et al. 2012). Maximum campaign GPS recorded uplift exceeded 13 cm (open star in Figure 3-4B) and several locations in eastern Christchurch (see closed stars in Figure 3-4B for examples) recorded subsidence > 10 cm (Beavan et al., 2012). Differential InSAR reveals areas where combined differential vertical and horizontal movements exceeded 10 cm (Beavan et al., 2012) and differential LiDAR reveals large areas of eastern Christchurch that subsided ≥ 10-20 cm.

The 23 December 2011 Mw 5.8 and Mw 5.9 earthquakes ruptured NE-striking reverse-right-lateral, blind faults primarily located offshore, shown in Figure 3-4B, with maximum slip of >1.4 m occurring at depths of 2-5 km and rupture extents of ~ 1 km depth (Beavan et al. 2012). Maximum campaign GPS recorded uplift of approximately 10 cm occurred along the eastern coast of Christchurch (open circle in Figure 3-4B); maximum subsidence occurred 5 to 8 km north of uplifted areas (closed circle in Figure 3-4B) (Beavan et al. 2012). Differential InSAR reveals areas where combined differential vertical and horizontal movements exceeded 5 cm

(Beavan et al., 2012). Differential LiDAR reveals continued subsidence exceeding 5 to 10 cm in eastern Christchurch.

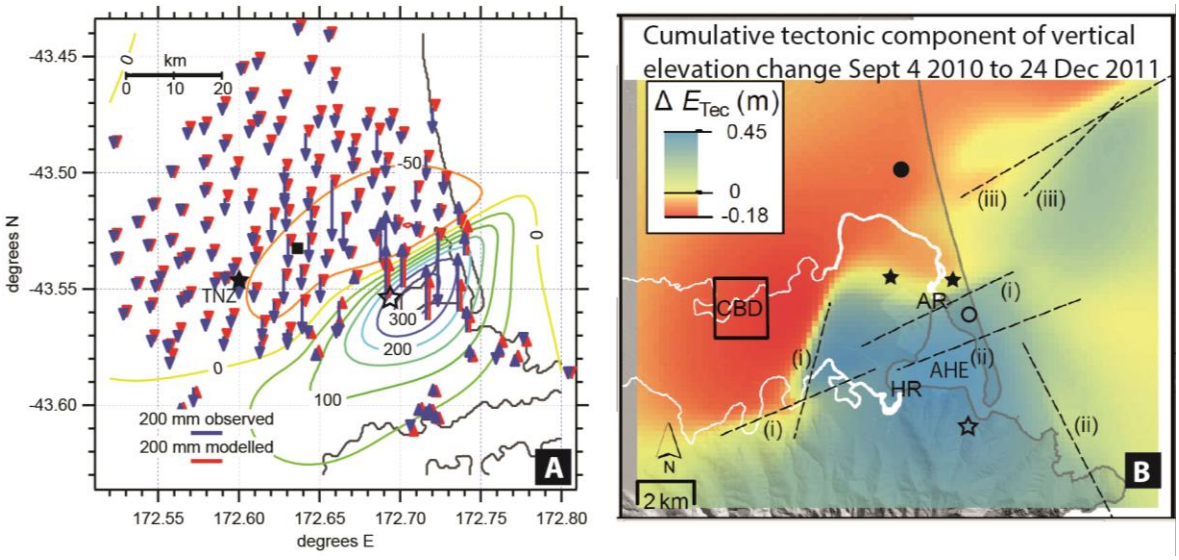

Figure 3-4 A) Vertical surface displacements in the 22 Feb Mw 6.2 Christchurch earthquake recorded by campaign GPS measurements ('observed') and modelled displacements from fault source models ('modelled') from Beavan et al. (2011). Contours of modelled vertical displacements shown in 50 mm increments. Location of cGPS station TNZ as shown. Site with maximum vertical uplift shown by open star. B) Tectonic component of cumulative vertical displacements (ΔE_{Tec}) in Christchurch and offshore, derived from fault source models of Beavan et al. (2012). The shaking-induced components of vertical deformation are not shown (see Figure 3-5). Up-dip surface projections of faults that ruptured in the 22 Feb (i), 13 June (ii), and Dec 23 (iii) earthquakes shown by dashed lines. See text for details.

The tectonic component of total measured vertical and horizontal displacements was derived from the fault source models of Beavan et al. (2012) (Figure 3-4A); van Ballegooy et al. (2014) used these models to extract the tectonic component in order to document the shaking-induced component of total subsidence (see next section). Hughes et al. (in review) combined the fault source models of Beavan et al. (2012) to produce a composite map showing the cumulative tectonic component of vertical displacements throughout the CES (Figure 3-4B). Three key observations can be made from this modeled displacement field in terms of potential tectonic influence on flooding in Christchurch: (1) The Avon River (AR; Figure 3-4B) has been influenced by cumulative tectonic subsidence throughout its reach, until it crosses the up-dip surface projection of one of the 22 Feb 2011 fault ruptures (Fault i; Figure 3-4B) where it enters the Avon-Heathcote Estuary (AHE in Figure 3-4B), (2) The Heathcote River (HR; Figure 3-4B) has been influenced by cumulative tectonic subsidence in its upstream reach and cumulative tectonic uplift in its downstream reach, with a change across the up-dip surface projection of another one of the 22 Feb 2011 fault ruptures (Fault i; Figure 3-4B), (3) The Avon-Heathcote Estuary (AHE) has been largely influenced by cumulative tectonic uplift throughout its spatial extent. The associated tectonically-induced gradient changes on the Heathcote River are

expected to increase flooding in the upstream reach, the tectonic uplift of the AHE is expected to increase flooding in both the Avon and Heathcote Rivers, and the tectonic influence on the Avon River is expected to lower the channel with respect to sea-level, and thus increased flood potential along the river.

Liquefaction induced settlement & lateral spreading

Liquefaction induced settlement was documented in Christchurch and the surrounding communities after the four events making up the 2010-2011 Canterbury earthquake sequence. Pre 2010 to post December 2011, elevation changes for the city were documented by Tonkin & Taylor (2013). Figure 3-5 shows cumulative settlements as a result of the four events in the Avon and Heathcote catchment areas. Cumulative settlements in excess of 1 m can be found within the Avon River catchment area. In the Heathcote catchment area both settlements and uplift of ≤ 0.3 m can be found. Van Ballegooy et al. (2014) found that > 87% of the settlement in Christchurch was associated with ejected soil.

GEER team members classified the ejected material as non-plastic fine sands and silty sands, during the Darfield Earthquake reconnaissance (NZ-GEER, 2010). Much of the silts and sands ejected due to liquefaction in the city were cleaned up after each of the events and placed in stock piles near the Bromley oxidation ponds and at the Burwood Landfill (NZ-GEER, 2011). Evidence of ejected material, as shown in Figure 3-6 was still found in Dudley Creek and along the banks of the Heathcote River near the high water marks during the GEER visit. CCC's Land Drainage Recovery Programme (2014) identified sediment volumes in excess of 350 truckloads have been removed since June of 2013 in ongoing attempts to restore channel morphology, and thus, flow capacity.

Lateral spreading damage within Christchurch was also documented in the previous two GEER reports (NZ-GEER 2010; NZ-GEER 2011) and subsequent publications, and is outside the scope of this report. Horizontal movement towards the center of the channel due to lateral spreading was documented throughout Christchurch and its surrounding communities in the previous GEER reports. This type of ground movement reduced the channel capacities and increased flood risk. Extensive mapping of the lateral spreading throughout the city was later conducted and presented by Tonkin & Taylor (2013). Figure 3-7 shows the mapped lateral spreading along the Avon River and resulting horizontal land movement.

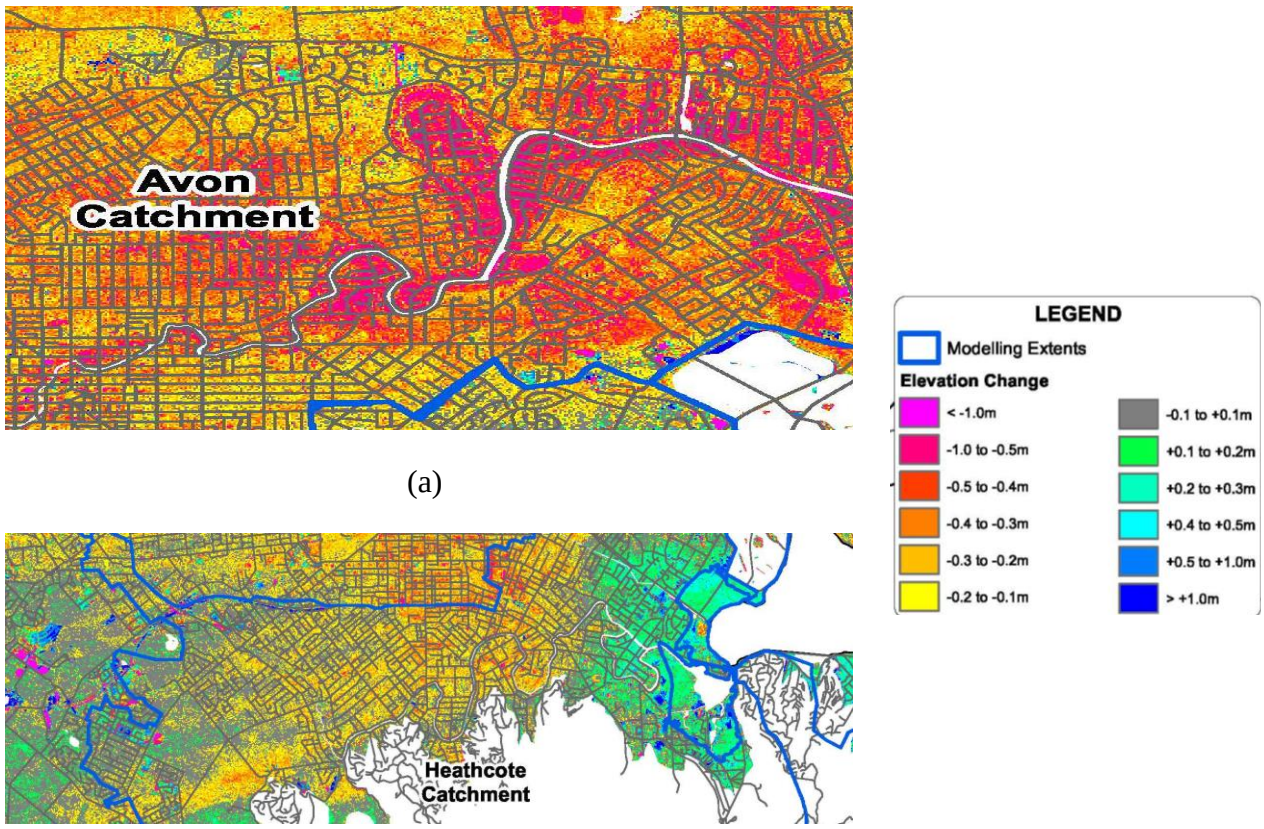

(a)

(b)

Figure 3-5 Cumulative elevation change along the Avon and Heathcote Rivers pre-2010 and post June/December 2011; (a) Avon Catchment and (b) Heathcote catchment. Maps (a) and (b) have different scales. (Tonkin & Taylor Ltd, 2013, Figure A10)

(a) (b)

Figure 3-6 (a) Traces of ejected sand in Dudley Creek (Stapletons Rd: -43.511154°, 172.655033°) and (b) similar sediments deposited during the March 5th Heathcote flooding (Centaurus Rd: -43.567442°, 172.645985°).

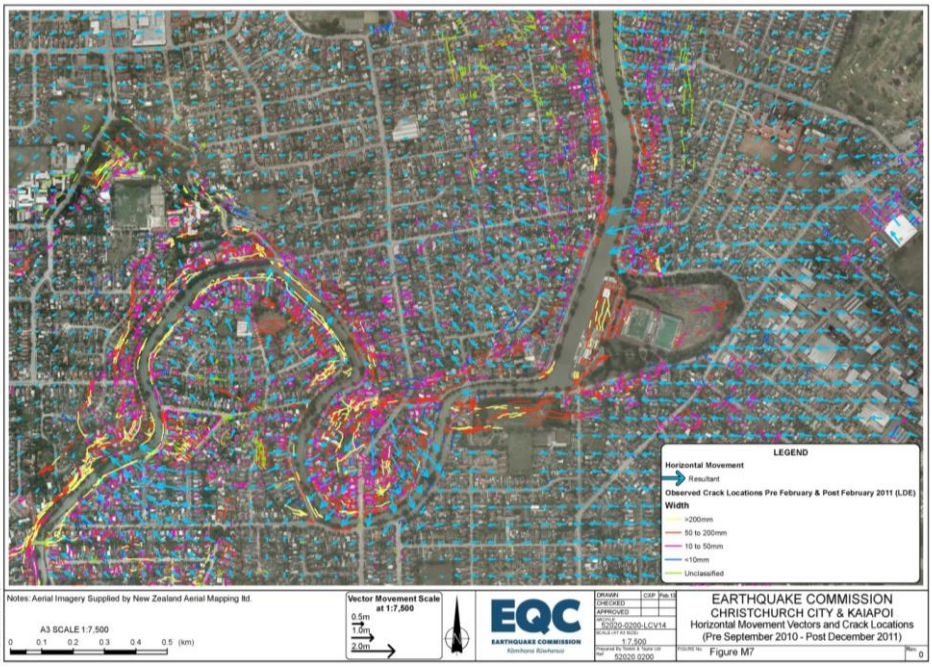

Figure 3-7 Lateral spreading and horizontal movement along the Avon River pre 2010 and post June/December 2011earthquakes (Tonkin & Taylor Ltd, 2013, Appendix M Figure 13)

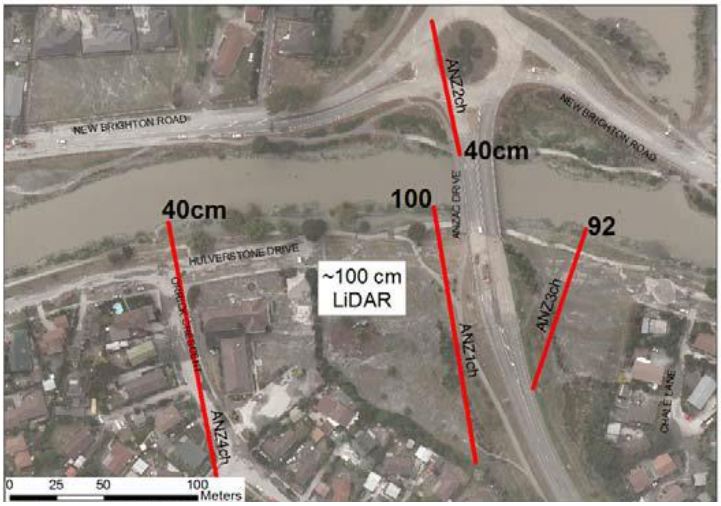

(a)

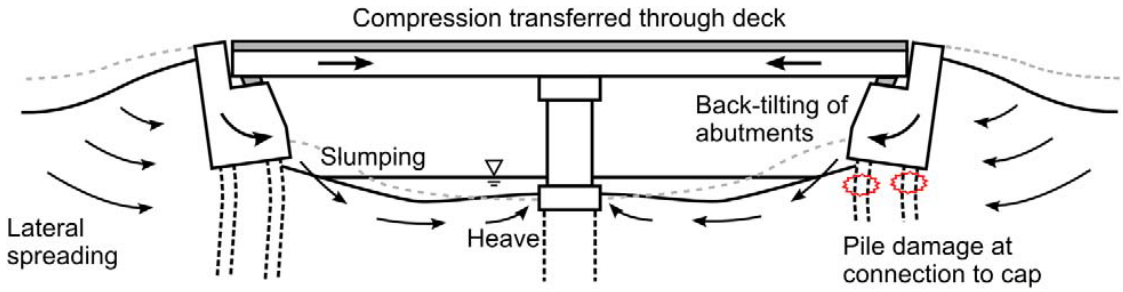

(b)

Figure 3-8 (a) Displacement of the river bank towards the center of the river at the Anzac Bridge and (b) example of lateral spread and slumping of bridge abutments creating loss of channel capacity from Cubrinovski et al. (2014)

Cubrinovski et al. (2014) show the collapse of the river banks in Figure 3-8a due to lateral spreading around the bridge foundations along the Avon River. The result is shown in Figure 3-8b as a narrowing of the channel from slumping of the sides and heave at the center as the two slumping sides come together.

Impacts and changes to river morphology

During the GEER team visits after the earthquakes in 2010 and 2011, liquefaction and lateral spreading have been documented at the rivers, as well as resulting bridge damages and bank failure (NZ-GEER 2010; NZ-GEER 2011). In the context of flood risk, such changes in general river morphology are of high interest (Neuhold et al., 2009).

The review of a time series of Google Earth images and aerial photos in Figure 3-9 gives a first insight into changes in river morphology. Regarding a short section of the Avon River in the vicinity of the Anzac Bridge, which suffered noticeable damages during the earthquake (NZ-GEER 2011), the river banks can be described as well-defined and distinguishable in the Google Earth image from March 2009. In the aerial photo (Canterbury Geotechnical Database, 2012) from September 2010 the northern banks of this section, in particular, are washed out and the river appeared to be widened. In 2011, this process appears to have increased slightly, while a shoal at the southern side of the river seems to be present.

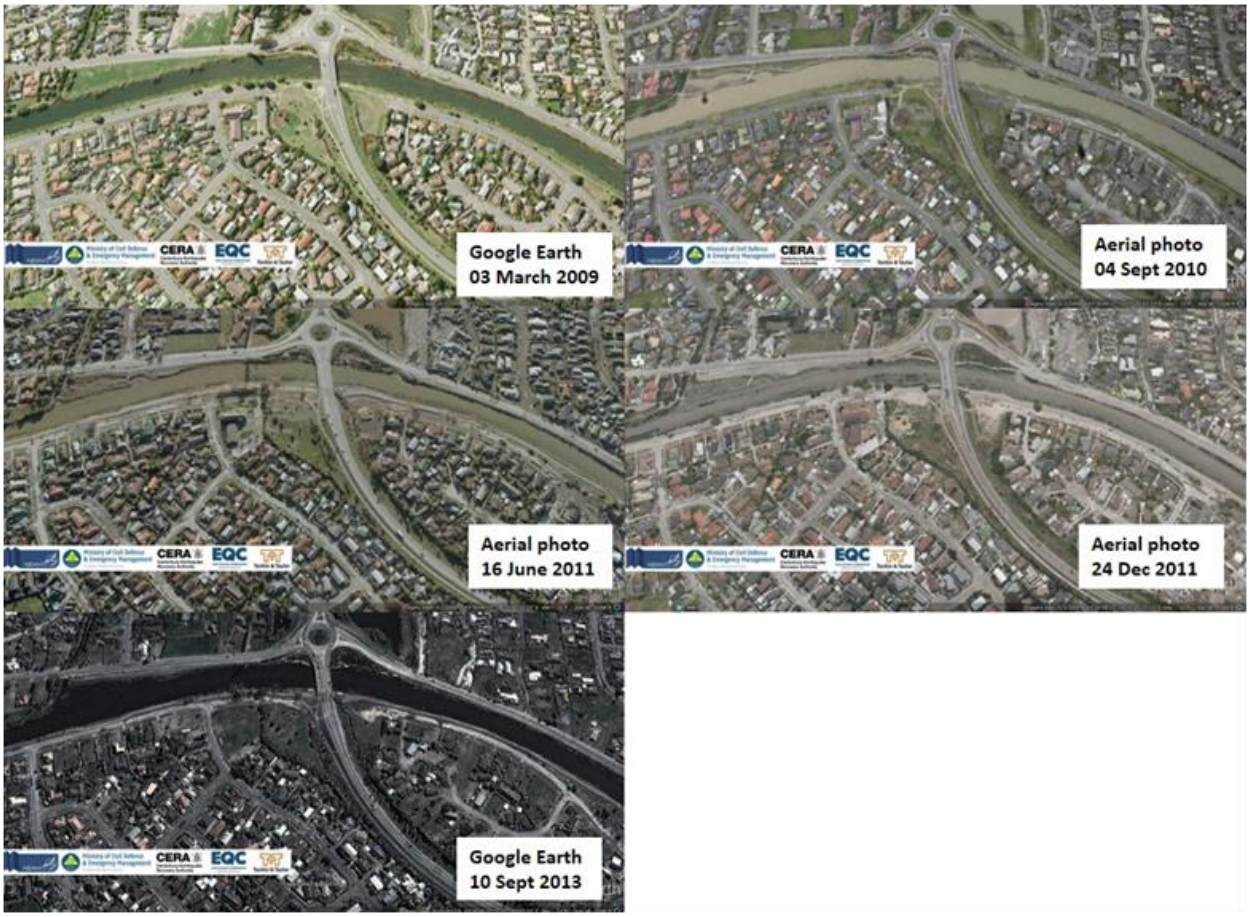

Figure 3-9 Time series of Google Earth images and aerial photos (Canterbury Geotechnical Database 2012) from March 2009 to September 2013 showing a short section of the Avon River in the vicinity of the Anzac Bridge (Anzac Drive: -43.500924°, 172.701084°).

More insights are given in a study by Tonkin & Taylor relating changes in river morphology to horizontal ground motion. In Figure 3-10, two Avon River cross-section topographies are shown. Both cross-sections represented sites at which major horizontal movement (>1.2 m) occurred. Cross-section 6 located between Avondale Bridge and Anzac Bridge is a rather narrow (ca. 22 m) and deep (~2.8 m in 2008) part of the Avon River, and was subject to significant earthquake-

induced infilling of the channel. This is expressed in a shallower water depth of ~1.8 m in 2011, and a decrease in slope of the submerged part of the banks, especially at the northern bank. Such decreases in cross-sectional area of the river potentially lead to higher water levels, higher flow speeds and a higher risk for overtopping of the banks during floods. Higher flow speeds can positively contribute to a natural deepening of the channel, but also to increased erosion and destabilization of the banks and scour, for example, at Anzac Bridge. Section 5 is crossing approximately between Horseshoe Lake Walk and Prestwick St. Here, the Avon is significantly wider (~60 m) with a water depth of ~1.8 m in 2008. Despite major horizontal movement, infill of the channel can only be observed at the eastern 25 m of the river, decreasing the water depth slightly to 1.2-1.6 m. As expected, the horizontal movement had less impact on this wider section of the river, likely leading to no relevant changes in flow conditions.

Four more cross-sections were examined in Figure 3-11 along the Avon River going upstream from the previous river section. Cross-section 4 is located between Ngarimu St and Gloucester St Bridge. In 2008, this cross-section was characterized by a width of ~24 m, a maximum water depth of ~1 m and shoal (water depth ~0.4 m) approximately in the center of the channel. This area was subject to significant horizontal movement southwards. This led to a shift of the northern bank narrowing the river to a width of ~20 m. Furthermore, the river depth decreased to a depth approximately equal to the depth of the previous shoal (~0.4 m). The deeper channel south of the shoal was entirely filled in, while the southern side of the channel steepened. Cross-section 3 is located approximately where Bowie Place turns off Avonside Drive, and was affected by significant horizontal movement pushing from both sides into the river. However, regarding river infill, the stronger southwestward movement clearly dominated and shifted the eastern bank about 3 m into the river, narrowing the river width to ~ 16 m. At the same time, the water depth was decreased from ~ 1 m to ~ 0.4 m. Cross-section 2 (approx. at the eastern end of Robson Abe) and cross-section 1 (just downstream of Banks Ave) were both mainly impacted by horizontal movement from the south/west. In both cases, the northern/north-eastern bank remained steady, while the southern/south-western bank was shifted by ~ 5 m into the river and the water depth at the deeper part of the channel decreased by ~ 0.5 m to 0 to 0.3 m. This confirmed the previous observation and expectation that the narrower river sections suffered more from horizontal movement, while the sediment contribution at wider section appeared rather insignificant.

After 2011, large sections of the rivers have been subject to dredging activities to restore the original river morphology and decrease flood risks associated with the smaller river cross-sectional areas (discussions with representatives of the Christchurch City Council). Dredging activities and post-dredging investigations of river morphology were overseen by the Christchurch City Council and confirmed the restoration of approximately pre-earthquake conditions at a large number of critical river sections. Specific data has not been published yet. According to these results, the increased flood risk at these rivers has likely been adequately

mitigated by restoring the river morphology to pre-earthquake conditions. New and improved dredging equipment will also ensure future stability of the river morphology.

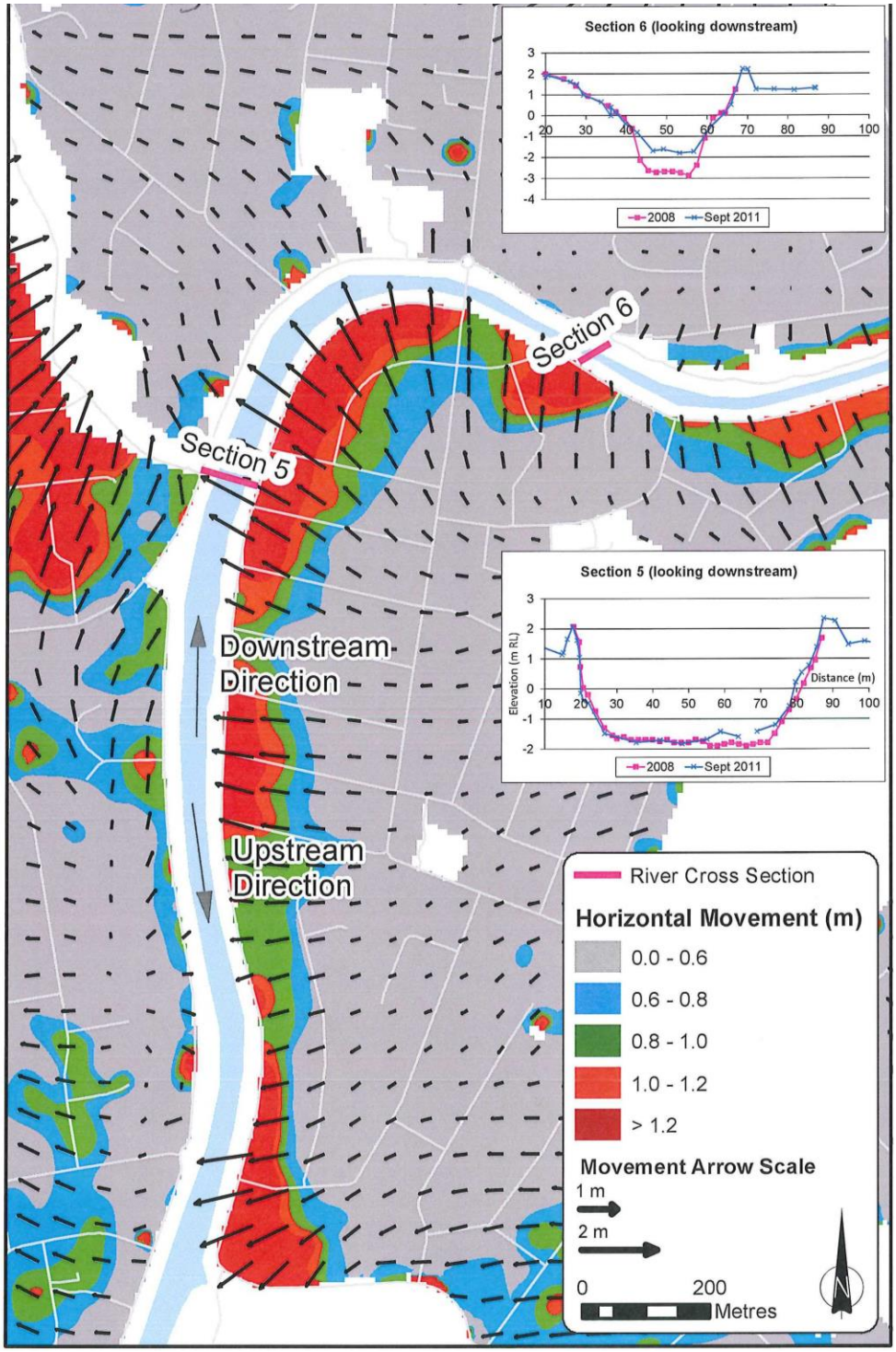

Figure 3-10 Map of earthquake induced horizontal ground movement along the Avon River section covering the area hugging Avonside Drive and a part of the Avon River between Avondale Bridge and Anzac Bridge (courtesy of Tonkin and Taylor), including the topographies of two river cross-sections in 2008 and September 2011.

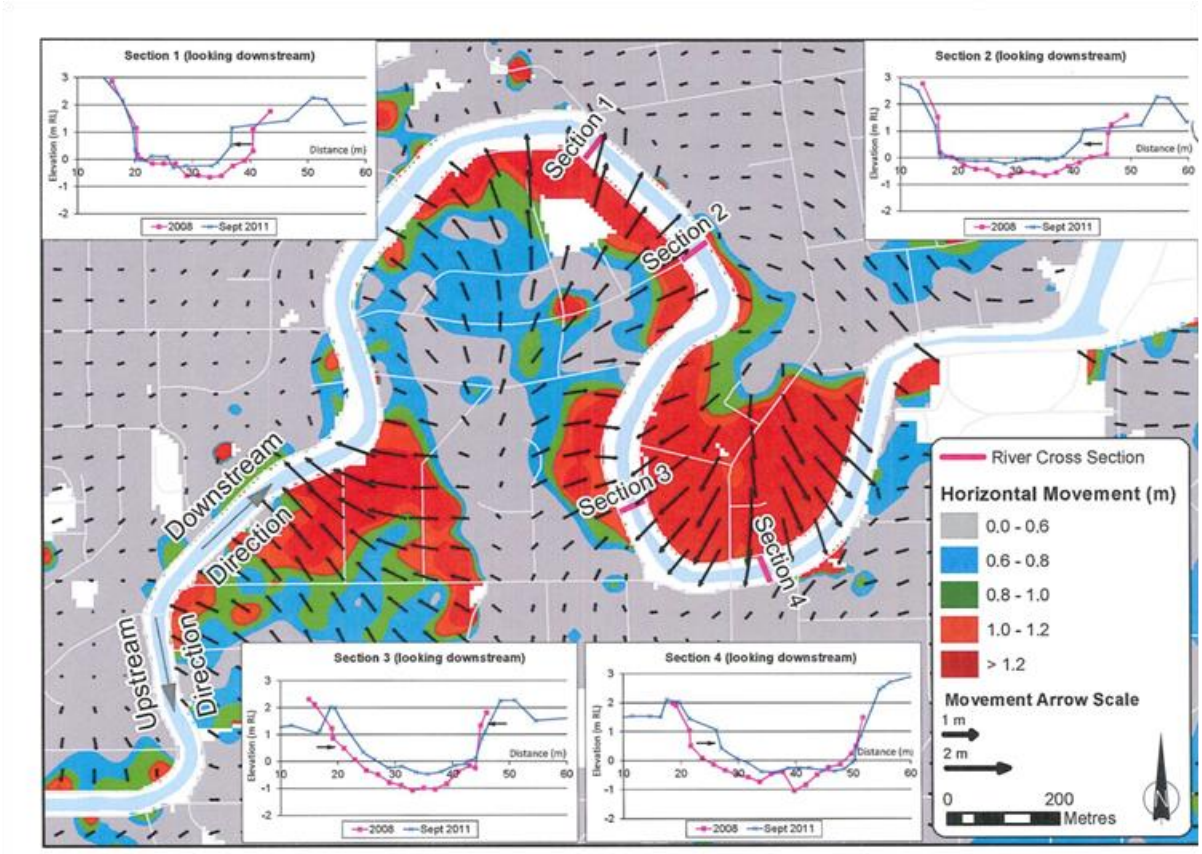

Figure 3-11 Map of earthquake induced horizontal ground movement along the Avon River section covering the area from Avonside Drive and to Stanmore Road Bridge (courtesy of Tonkin and Taylor), including the topographies of four river cross-sections in 2008 and September 2011.

Improvements and specifying LiDAR

Aerial LiDAR surveys proved extremely beneficial for post-earthquake geotechnical and hydrological evaluations. The CES provided a unique opportunity to use LiDAR in a new capacity. As a result, this section describes some areas where LiDAR was successfully used to great benefit and lessons learned for improving LiDAR use in the future.

While aerial photography is a valuable resource, there is little doubt that the detailed topographic information provided by the aerial LiDAR has both accurately quantified and provided valuable insights into the ground surface movements during the CES. The engineering and insurance communities have already benefited immensely from understanding and quantifying the ground surface and how it has changed, and the scientific community will no doubt continue to mine this rich data source.

A significant portion of the value derived from the Christchurch LiDAR data relied on LiDAR surveys for hydrological modeling that were commissioned by local government agencies before the 4 September 2010 Darfield Earthquake. While Christchurch was subjected to a sequence of

earthquakes, and would have still benefited had the LiDAR data acquired one day after that first earthquake been the only survey available, these hydrological surveys provided important baseline information to quantify movements during that first earthquake.

A serendipitous benefit of the hydrological LiDAR surveys was that they covered a significantly greater area than could be justified for the 5 September 2010 LiDAR, which was primarily for emergency management purposes. Subsequent surveys were commissioned with greater extents, particularly once the value of LiDAR was more widely appreciated within the insurance and engineering communities and once this benefit was realized by central government agencies able to fund such data gathering efforts. While their principal uses to date have been quantifying land damage (e.g. subsidence, lateral spreading and increased flood vulnerability), they are an invaluable resource for identifying and devising remediation solutions for both widespread and localized areas of change.

The surveys later in the earthquake sequence aimed to provide better topographical accuracy by acquiring the LiDAR once liquefaction ejecta was judged to be mostly removed from the ground surface (and either piled in streets or trucked away). This contrasts with aerial photography that was more usefully flown as soon as practicable after the earthquake in order to record the extents of liquefaction ejecta.

While baseline LiDAR surveys are invaluable for identifying elevation changes after significant earthquake events, the Christchurch experience indicates that they need to be regularly updated in any area being monitored. While an obvious purpose of this is to record changes in land use, capturing the pre- and post-event point clouds using similar instruments maximizes the value of the post-event data because the earlier data will have similar precision, accuracy and point density. Short time intervals between surveys also allows for more certainty in isolating earthquake induced changes from background geomorphic dynamics. The Christchurch coast dunes, for example, had grown significantly via aeolian processes between the pre-quake 2003 LiDAR survey and the first post-quake survey, making the determination of exact earthquake-induced deformation of the shore-proximal coastal plain impossible.

A third driver for regular pre-earthquake updates is data retention. While the 2003 LiDAR point cloud was stored in a format that was easily revised 8 years later to use an improved geoid offset model published in 2009, only the thinned ground returns had been retained. This could be because only that subset of the data, which was still a reasonable portion of the capacity of a hard disk in 2003, was regarded as valuable enough to maintain in an accessible format. Periodic updates could maintain an active interest in using the data and thereby ensure it is well curated from machine to machine and person to person.

Publication of one form of LiDAR on the Canterbury Geotechnical Database (CGD), in a format that is almost universally accessible without specialized Geographical Information Systems knowledge or (expensive) software, has also helped the engineering community understand what

it is and how it can be used. Publishing LiDAR in an equally accessible format in areas that could be subject to extreme ground level altering events, including earthquakes, cliff collapses, and landslides, would not only go some way toward encouraging regular LiDAR updates, but would ensure that the local engineering community understand its value and frequently use it well before they need to use it for emergency response purposes.

Most mapping in the CGD and large scale analysis has relied on Digital Elevation Models (DEM) defined by averaging the ground surface elevations within 5 m square cells rather than the full point clouds. This cell size appears to be the best compromise between increasing the number of returns in each cell to improve the accuracy and minimize the cell size to provide an adequate representation of the variation in surface elevations.

The number of cell returns was particularly important for the DEM constructed from the sparser 2003 (hydrological) LiDAR, but also provided DEMs that were reasonably easily stored and processed. Ideally, water penetrating LiDAR instruments should be used in areas with significant waterway, coastal and/or estuarine features. In Christchurch the earlier LiDAR surveys were non-water penetrating, limiting the ability to detect elevation changes across the Avon-Heathcote Estuary Ihuati. Boat and ground based surveys were used to determine that two thirds of this feature had been uplifted but the coverage of these surveys, which were completed using grids and transects, was not as thorough as could have been provided using water penetrating LiDAR.

A reasonable amount of effort was expended to verify the accuracy of the LiDAR (CERA, 2014). This showed that the accuracy of each entire LiDAR point cloud is close to the accuracy of New Zealand's geoid offset model, representing the difference between GPS-based and precise leveling surveys. However there was better precision available within localized subsets of the point cloud (e.g. hard surfaces such as streets). The verification benefited from a good source of surveyed reference benchmarks. Benchmarks on the ground surface were more easily compared with the LiDAR point cloud than those buried below (often not well defined distances below the ground surface).

Most Christchurch properties appeared to have an adequate portion of their total area visible to the LiDAR scanner (i.e. uncovered by structures or obscured by vegetation) to provide adequate representations of the ground surface elevations. Similarly, while seasonal vegetation differences didn't appear to have much observable effect on the DEMs for Christchurch, this could be an issue in more densely vegetated or built up urban areas.

Finally, horizontal ground movements were estimated by correlating elevations within pairs of DEMs. This required a significant amount of work to remove systematic noise that produced chessboard-like patterns in larger areas than those illustrated in the Figure 3.1 elevation differences. A significant recommendation resulting from this analysis was that LiDAR flight paths need to be reasonably similar to provide better estimates of horizontal movements.

References

Beavan, J., Wallace, L., Samsonov, S., Ellis, S., Motagh, M., & Palmer, N. (2010). The Darfield (Canterbury) earthquake: geodetic observations and preliminary source model. Bulletin of the New Zealand Society for Earthquake Engineering, 43(4), 228.

Beavan, J., Fielding, E., Motagh, M., Samsonov, S., & Donnelly, N. (2011). Fault location and slip distribution of the 22 February 2011 Mw 6.2 Christchurch, New Zealand, earthquake from geodetic data. Seismological Research Letters, 82(6), 789-799.

Beavan, J., Motagh, M., Fielding, E. J., Donnelly, N., & Collett, D. (2012). Fault slip models of the 2010–2011 Canterbury, New Zealand, earthquakes from geodetic data and observations of postseismic ground deformation. New Zealand Journal of Geology and Geophysics, 55(3), 207-221.

Bradley, B. A., Quigley, M. C., Van Dissen, R. J., & Litchfield, N. J. (2014). Ground motion and seismic source aspects of the Canterbury earthquake sequence. Earthquake Spectra, 30(1), 1-15.

CERA (2014) Verification of LiDAR acquired before and after the Canterbury Earthquake Sequence. Canterbury Geotechnical Database Technical Specification 03, 30 April 2014 (available https://canterburygeotechnicaldatabase.projectorbit.com/)

Christchurch City Council (2014) Land Drainage Recovery Program Presentation Avon Otakaro Canterbury Geotechnical Database (2012). Aerial Photography, Map Layer CGD0100-1 June 2012

Cubrinovski, M., Winkley, A., Haskell, J., Palermo, A., Wotherspoon, L., Robinson, K., ... & Hughes, M. (2014). Spreading-Induced Damage to Short-Span Bridges in Christchurch, New Zealand. Earthquake Spectra, 30(1), 57-83.

Cubrinovski, M., Green, R.A., Wotherspoon, L., Allen, J., Bradley, B., Bradshaw, B., Bray, J., DePascale, G., Orense, R., O'Rourke, T., Pender, M., Rix, G., Wells, D. & Wood, C. (2011). Geotechnical reconnaissance of the 2011 Christchurch (New Zealand) earthquake. Geotechnical Extreme Events Reconnaissance (GEER) Association Report no. GEER-027.

Duffy, B., Quigley, M., Barrell, D. J., Van Dissen, R., Stahl, T., Leprince, S., ... & Bilderback, E. (2013). Fault kinematics and surface deformation across a releasing bend during the 2010 MW 7.1 Darfield, New Zealand, earthquake revealed by differential LiDAR and cadastral surveying. Geological Society of America Bulletin, 125(3-4), 420-431.

Green, R. A., Cubrinovski, M., Cox, B., Wood, C., Wotherspoon, L., Bradley, B., & Maurer, B. (2014). Select Liquefaction Case Histories from the 2010-2011 Canterbury Earthquake Sequence. Earthquake Spectra, 30(1), 131-153.

Green, R.A., Cubrinovski, M., Allen, J., Ashford, S., Bowman, E., Bradley, B., Cox, B., Hutchinson, T., Kavazanjian, E., Orense, R., O'Rourke, T., Pender, M., Quigley, M. & Wotherspoon, L. (2010). Geotechnical reconnaissance of the 2010 Darfield (New Zealand) earthquake. Geotechnical Extreme Events Reconnaissance (GEER) Association Report no. GEER-024.

Hughes, M., Quigley, M., van Ballegooy, S., Deam, B., Bradley, B., Hart, D., Measures, R. (in review). The sinking city: Earthquakes increase flood hazard in Christchurch, New Zealand, GSA Today.

Kaiser, A., Holden, C., Beavan, J., Beetham, D., Benites, R., Celentano, A., ... & Zhao, J. (2012). The Mw 6.2 Christchurch earthquake of February 2011: preliminary report. New Zealand journal of geology and geophysics, 55(1), 67-90.

Li, Y. G., De Pascale, G. P., Quigley, M. C., & Gravley, D. M. (2014). Fault damage zones of the M7. 1 Darfield and M6. 3 Christchurch earthquakes characterized by fault-zone trapped waves. Tectonophysics, 618, 79-101.

Maurer, B., Green, R., Cubrinovski, M., and Bradley, B. (2014). "Evaluation of the Liquefaction Potential Index for Assessing Liquefaction Hazard in Christchurch, New Zealand." *J. Geotech. Geoenviron. Eng.* , 10.1061/(ASCE)GT.1943-5606.0001117 , 04014032.

Neuhold, C., Stanzel, P., & Nachtnebel, H. P. (2009). Incorporating river morphological changes to flood risk assessment: uncertainties, methodology and application. *Natural Hazards & Earth System Sciences*, *9*(3).

Quigley, M., Villamor, P., Furlong, K., Beavan, J., Van Dissen, R., Litchfield, N., ... & Cox, S. (2010). Previously unknown fault shakes New Zealand's South Island. EOS, Transactions American Geophysical Union, 91(49), 469-470.

Quigley, M., Van Dissen, R., Litchfield, N., Villamor, P., Duffy, B., Barrell, D., ... & Noble, D. (2012). Surface rupture during the 2010 Mw 7.1 Darfield (Canterbury) earthquake: Implications for fault rupture dynamics and seismic-hazard analysis. Geology, 40(1), 55-58.

Quigley, M. C., Bastin, S., & Bradley, B. A. (2013). Recurrent liquefaction in Christchurch, New Zealand, during the Canterbury earthquake sequence. Geology, 41(4), 419-422.

Quigley, M., Hughes, M., Bradley, B., van Ballegooy, S., Reid, C., Morgenroth, J., Horton, T., Duffy, B., (in review). Environmental impacts of the 2010-2012 Canterbury earthquake sequence: defining the geologic legacy of clustered earthquakes sourced primarily from blind faults. Tectonophysics.

Tonkin & Taylor Ltd (2013). Liquefaction vulnerability study. Earthquake Commission. T&T Ref: 52020.0200/v1.0.

Van Ballegooy, S., Malan, P., Lacrosse, V., Jacka, M. E., Cubrinovski, M., Bray, J. D., ... & Cowan, H. (2014). Assessment of liquefaction-induced land damage for residential Christchurch. Earthquake Spectra, 30(1), 31-55.